Plankton Benthos Res 20(1): 1–11, 2025

Plankton & Benthos Research

Quantitative evaluation of *Karenia* cells using FlowCam: Applying to its distribution in Hidaka Bay, southern Hokkaido, northern Japan during autumn 2022

Hikaru Kubo[1], Takahiro Iida[1], Keiri Imai[1], Atsushi Ooki[1,2] & Kohei Matsuno[1,2,*]

[1] *Faculty/Graduate School of Fisheries Sciences, Hokkaido University, 3–1–1 Minato-cho, Hakodate, Hokkaido 041–8611, Japan*
[2] *Arctic Research Centre, Hokkaido University, Kita-21 Nishi-11 Kita-ku, Sapporo, Hokkaido 001–0021, Japan*

Received 24 May 2024; Accepted 26 September 2024 Responsible Editor: Akihiko Tuji

doi: 10.3800/pbr.20.1

Abstract: Since 2015, occurrences of *Karenia* spp. blooms have been documented in Hakodate Bay, potentially expanding to the Pacific coastal area of Hokkaido via the Tsugaru Warm Current. However, available information on the expanding distribution remains limited. This study aims to elucidate the distribution of *Karenia* spp. in Hidaka Bay, which is an area downstream of the Tsugaru Warm current from Hakodate Bay, using image analysis technology, specifically the FlowCam, following a comprehensive quantitative assessment to facilitate cell detection. The FlowCam could detect *Karenia* spp., with assured quantitative precision when the cell density exceeds 1 cell mL^{-1}. Counting resulted in lower calculated densities that varied widely, suggesting potential subsampling biases. Using the FlowCam's software enabled image filtration of *Karenia* spp. from other plankton species with a maximum accuracy of 96%. Optimal filtering performance in the software was achieved through a combination of Equivalent Spherical Diameter, Aspect Ratio, and Average Green values. Despite a loss of ~10% of *Karenia* spp. images using the filter function, the application of this function significantly reduces the effort required for the cell sorting-out process. Field observations conducted in September 2022 revealed the presence of *Karenia* spp. across all stations in Hidaka Bay and Hakodate Bay. Furthermore, the observed gradient in cell density from the warmer waters of Hakodate Bay towards Hidaka Bay suggests the potential role of the Tsugaru Warm Current in facilitating transportation of *Karenia* spp. cells into Hidaka Bay.

Key words: Accuracy, Automatic elimination, Filter function, *Karenia mikimotoi*

Introduction

Karenia spp. are harmful and toxic dinoflagellates, and blooms caused by *Karenia mikimotoi* can lead to substantial financial losses to marine aquaculture operations (Li et al. 2017). This species has primarily been distributed along the coast of western Japan (Matsuoka et al. 1989), frequently causing red tides in northern Kyushu and the Seto Inland Sea, causing substantial damage to fisheries (Imai et al. 2006, Nishiyama et al. 2013). However, in 2015, an unprecedented occurrence of *K. mikimotoi* red tide was documented in Hakodate Bay, situated in southern Hokkaido (Shimada et al. 2016). It has been suggested that this occurrence may be attributed to the transportation of cells by the Tsugaru Warm Current from Hakodate Bay to the Pacific coastal area of Hokkaido (Shimada et al. 2016). However, there have been no reports revealing *K. mikimotoi* occurrence in the Tsugaru Warm Current.

The Tsugaru Warm Current flows from the Japan Sea into the Tsugaru Straits, directly impacting Hakodate Bay with warm, saline seawater (Yasui et al. 2022). The average volume transport of the Tsugaru Warm Current is approximately 1.5 Sv and is linked to the difference in sea level between the Japan Sea and the Pacific Ocean (Ito et al. 2003). Seasonally, the current's trajectory shifts between a "gyre mode" and a "coastal mode" (Conlon 1982). The gyre mode predominates during summer and autumn, and is characterized by a clockwise gyre extending to 143°E, whereas the coastal mode prevails during winter

* Corresponding author: Kohei Matsuno; E-mail, k.matsuno@fish.hokudai.ac.jp
Supplementary materials may be found in the online version of this article.

and spring, and is confined to a narrower expanse along the Honshu coastline (Conlon 1982). It is hypothesized that *Karenia* spp., responsible for red tides in Hakodate Bay, are conveyed by the Tsugaru Warm Current to the Pacific coast of Hokkaido, including Hidaka Bay. However, limited research has been conducted on phytoplankton dynamics within this region.

Phytoplankton observations traditionally rely on labor-intensive microscopic cell counting methods, which are susceptible to inaccuracies stemming from observer fatigue (Buskey & Hyatt 2006). However, recent advancements in image analysis technology have introduced efficient alternatives, such as the FlowCam (Sieracki et al. 1998) imaging FlowCytobot (Olson & Sosik 2007) and PlanktoScope (Pollina et al. 2022). Notably, the FlowCam has been extensively developed over 20 years and has been used across a variety of research studies (Owen et al. 2022). Capable of rapidly capturing high-speed images of particles within samples, the FlowCam expedites the analysis of nano- and micro-sized plankton while minimizing processing time. Moreover, through the use of the VisualSpreadsheet (or Classifier Advanced) filter function, a feature integrated into the FlowCam software, users can automatically select similar images from large datasets. Previous studies have reported the efficacy of automated classification for diatom species of various shapes, achieving filter accuracies exceeding 90% (Camoying & Yñiguez 2016; see Materials and Methods for details). Cyanobacteria, responsible for blue-green algae in freshwater, form colonies whose morphological characteristics are used for classification purposes rather than species identification (e.g., Saker et al. 1999). Taking advantage of this property, the FlowCam's filtering function has exhibited comparable classification accuracy to human observers in mesocosm experiments involving multiple cyanobacterial morphotypes, such as *Microcystis* spp. (Mirasbekov et al. 2021). Thus, the automated classification function can be used effectively by adjusting the target organisms and observation conditions. However, the current filter functions in the software have not been used in almost all previous studies (89%, cf. Owen et al. 2022). Additionally, more recent studies have explicitly explored machine learning functions (not filter function), which calculates a percent similarity between a target photo and some training images, for toxic and harmful algae, including *Karenia* spp. (Buskey & Hyatt 2006). Due to this, information regarding their application with regard to detecting *Karenia* cells using current filter functions in the VisualSpreadsheet remains scarce.

In this study, seawater samples were collected from Hidaka Bay, situated along the Pacific coast of Hokkaido, Japan, during the autumn of 2022. These samples were used to explore the optimal parameters for the automated classification of *Karenia* spp. using FlowCam. Note that we treated the *Karenia* cells as spp. due to the low-resolution quality of the images derived by the FlowCam, but used microscopic observations to confirm the cells as *Karenia mikimotoi* (cf. Fig. 1a, b). Through comparative analysis of obtained cell densities with hydrological and environmental data, our aim was to identify the ecological conditions conducive to *Karenia* spp. proliferation as well as to elucidate mechanisms facilitating their transportation into the Pacific coastal region of Hokkaido.

Materials and Methods

Field sampling

Field sampling was conducted aboard the T/S *Oshoro-Maru* and T/S *Ushio-Maru* vessels from the 15th to 18th, September 2022, along the Pacific coast of Hokkaido (41°37.8′ N–42°13.4′ N, 140°40.7′ E–143°39.7′ E) (Supplementary Table 1). Before sampling, red tides of *K. mikimotoi* were observed around Hakodate Bay in early September 2022 (Natsuike et al. 2023). During the T/S *Oshoro-Maru* cruise, surface seawater samples were obtained by pumping 1 L of water from the ship's bottom (7 m depth) at 27 stations along the route. These samples were fixed for phytoplankton samples by adding 25% glutaraldehyde to obtain a final concentration of 1%. Simul-

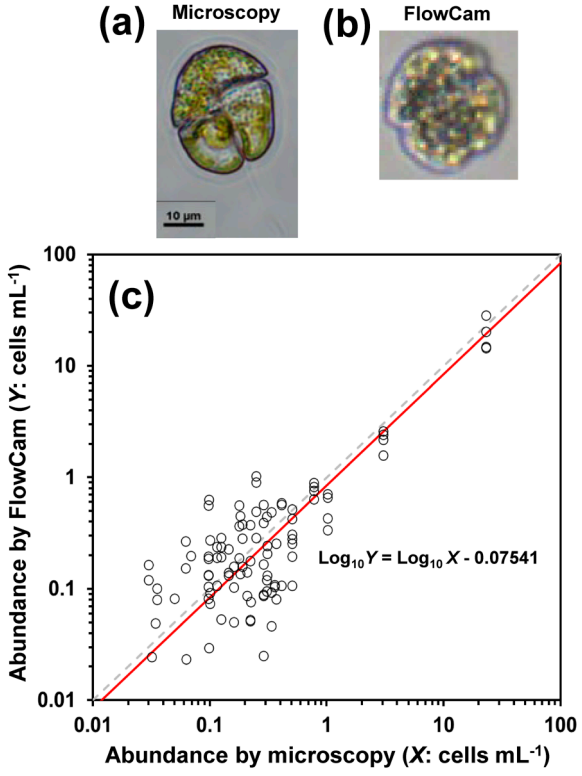

Fig. 1. Photo of *Karenia* taken by a camera (DS-Fi3, Nikon) using an inverted microscopy (a) and taken by the FlowCam (b). Comparison of cell density in *Karenia* spp. measured by microscopy and FlowCam (c). The red solid line indicates the regression between microscopy and FlowCam. The grey dashed line shows 1 : 1.

taneously, additional seawater samples were collected in 10 mL spit tubes and frozen for subsequent nutrient analysis. Throughout the cruise, the surface seawater analyzer provided continuous measurements of water temperature, salinity, *in-vivo* chlorophyll fluorescence, and turbidity using a T-S sensor (ACTW, JFE Advantech) and Chl-Turbidity sensor (ACLW, JFE Advantech). In addition, a red tide sensor (HAI sensor, JFE Advantech) (Yoshida et al. 2021) was placed in a tank containing continuously flowing seawater, recording the Fluorescence Spectral Shift Index (FSI) measurements at the time of each sample collection. The FSI is defined as the ratio of fluorescence intensities at two different wavelengths (670 and 690 nm) to represent the degree of fluorescence spectrum shifts (Yoshida et al. 2021). Additionally, the T/S *Ushio-Maru* cruise exclusively collected phytoplankton samples near the coastline of Cape Erimo.

Furthermore, seawater samples were collected using Niskin bottles from 10, 20, 30, 50, and 100 m at three stations during the T/S *Oshoro-Maru* cruise. Preservation of phytoplankton and nutrient samples followed the aforenoted protocol. Concurrently, a Conductivity-Temperature-Depth meter (CTD) (SBE911 plus, Sea-Bird Electronics Inc.) facilitated the acquisition of vertical profiles of water temperature, salinity, and fluorescence values.

Sample analysis

In the land laboratory located at the Hakodate campus of Hokkaido University, nutrient samples were measured for nitrate, nitrite, ammonium, phosphate, and silicate concentrations using an autoanalyzer (QuAAtro 2HR, BL-TEC).

Fixed samples (1 L) from the surface and vertical collections intended for counting *Karenia* spp. (by microscope and FlowCam) were concentrated by siphoning to a final volume of 15.1–19.4 mL (Sukhanova 1978). From this concentrated sample, a 500-μL aliquot was extracted onto a glass slide using a micropipette, and *Karenia* spp. were counted using an inverted microscope (ECLIPSE Ts2R, Nikon) at 200 to 400× magnification, using phase contrast. The number of cells counted in each sub-sample ranged from 0 to 146 cells. Because we concentrated a volume of 1 L into 15.1–19.4 mL, the limit of detection was 30.15–38.81 cells L^{-1} (0.0302–0.0388 cells mL^{-1}).

Following microscopic counting, the concentrated samples were analyzed by FlowCam (FlowCam 8100, Yokogawa Fluid Imaging Technologies, Inc.). The FlowCam was equipped with a 10× objective lens, a flow cell (FOV100, depth 100 μm, width 700 μm), and a 1 mL syringe. Operational software used in the FlowCam was VisualSpreadsheet6 (Yokogawa Fluid Imaging Technologies, Inc.). Prior to sample measurement, the camera focus was calibrated using microbeads (14.97 $\pm$ 0.12 μm). Subsequent to focus adjustment, each concentrated sample was taken using a micropipette, and the sample was placed into a 1 mL microtip inserted into the FlowCam sample inlet. The amount of concentrated sample dispensed by the micropipette was 0.5 mL and 1 mL for testing how much volume was required for quantitative subsampling. Images of particles in the concentrated sample were then taken in AutoImage mode. Measurements were conducted four times for each sample (two different volumes * two). Throughout the measurement process, the flow rate was maintained at 0.140 mL min^{-1}, with an acquisition rate set at 20 times per second, resulting in approximately 70% efficiency in imaging the sample volume. Due to this efficiency, the fluid volume imaged was 0.35 mL and 0.70 mL in the case of a total sample volume of 0.50 and 1 mL. Advanced acquisition filters were configured to automatically exclude unsuitable images (e.g., out of focus, too small/large), with thresholds set as < 10 and > 1000 μm for Equivalent Spherical Diameter (ESD) and < 40 for Edge gradient. The measurement was terminated when the sample in the microchip finished flowing. Duplicate and non-*Karenia* spp. images were removed from the images to obtain the number of cells of *Karenia* spp. Finally, cell density (cells mL^{-1}) was calculated by dividing the cell count by the fluid volume imaged (mL) analyzed with the FlowCam. Detection limits for FlowCam were 43.1–55.4 cells L^{-1} (0.0431–0.0554 cells mL^{-1}) using the 0.5 mL sample, and 21.5–27.7 cells L^{-1} (0.0215–0.0277 cells mL^{-1}) using the 1 mL sample.

Image analysis with FlowCam

A dataset comprising 50 images of *Karenia* spp. and 950 images of non-*Karenia* spp. was compiled from the image data obtained from the FlowCam (Supplementary Fig. 1). Additionally, a library containing 100 images of *Karenia* spp. was created. To create the library, both frontal-facing cells and non-frontal-orientation cells were included to set to filter out sufficient cells from natural samples. From this library, 31 filters were generated by combining five different properties: ESD, Aspect Ratio (the ratio of the major and minor axes of an ellipse centered on the particle's center of gravity), Average Green (the average intensity of green in the particle image [0–255]), Circle fit (the deviation of the particle contour from a perfect circle [perfect circle: 1]), and Perimeter (the length of the particle contour excluding the holes). Each filter was subsequently applied to the aforementioned dataset, containing 1000 images, to extract *Karenia* spp. images using the filter function embedded in the software. The software provides two filter functions: a value filter, which can be defined by minimum and maximum values, and a statistical filter, which can be defined by minimum, maximum, average, and standard deviation values. To test the best combination of the filter parameters, we used the value filter function. The number of images identified as *Karenia* spp. by each filter was recorded, and *Karenia* spp. and non-*Karenia* spp. images within these selections were visually identified and counted. Using these numbers of detections, Accuracy (Acu, %)—the percentage of *Karenia* spp. images among the extracted images, and True Accuracy (TAcu, %)—the actual per-

centage of *Karenia* spp. images among all detections (i.e., 1000 images)—were calculated using the following equations:

$$\mathrm{Acu} = N\_cor/50*100$$
$$\mathrm{TAcu} = N\_cor/Ni*100$$

where *Ni* represents the total number of images identified as *Karenia* spp. by the filter under a given condition *i*, and *N_cor* denotes the number of images within *Ni* that were visually confirmed as *Karenia* spp.

Furthermore, Filter Accuracy (FAcu, %) was calculated following Camoying & Yñiguez (2016), expressed as:

$$\mathrm{FAcu} = \frac{\text{True Positive} + \text{True Negative}}{\text{False Positive} + \text{False Negative} + \text{True Positive} + \text{True Negative}} * 100$$

where True Positive (synonymous with *N_cor*) represents the number of *Karenia* spp. images accurately identified as such, True Negative is the number of non-*Karenia* spp. images correctly determined as not belonging to *Karenia* spp., False Positive denotes the number of non-*Karenia* spp. images incorrectly classified as *Karenia* spp., and False Negative indicates the number of *Karenia* spp. images incorrectly determined as not belonging to *Karenia* spp.

Statistical analysis

To elucidate the relationship between environmental factors (including water temperature, salinity, and fluorescence) and *Karenia* spp. cell density as determined by microscopy, a distance-based redundancy analysis (dbRDA) was performed. Data from the surface and vertical sampling were used. To remove multicollinearity among the environmental factors, variance inflation factors (VIF) (Zuur et al. 2009) were calculated. Because all VIF values were below 5, none of the factors were removed for the subsequent analysis. Prior to the redundancy analysis, environmental data were standardized, and a resemblance matrix based on Euclidean distance was calculated. The dbRDA was performed using Primer 7 software (PRIMER-E Ltd.). Furthermore, to discern the optimal environmental conditions for *Karenia* spp., a decision tree analysis was performed using both *Karenia* spp. cell density data obtained via microscopy and environmental parameters (comprising water temperature, salinity, fluorescence, turbidity, and FSI). This analysis was performed using "rpart" and "partykit" packages within the R statistical computing environment (version 4.1.2, R Core Team, 2021).

Results

Comparison between microscope and FlowCam

Under the microscope, the *Karenia* cells were identified as *Karenia mikimotoi*, but we were unable to identify these using as such photos derived by the FlowCam (Fig. 1a, b). The cell density of *Karenia* spp. ranged from 0 to 23.2 cells mL^{-1} quantified by microscopy, and 0 to 28.4 cells mL^{-1} when quantified using the FlowCam. Preliminary observations from both microscopy and FlowCam showed a positive correlation between cell densities, as depicted by the equation: Log_{10} Y (cell density with FlowCam) = Log_{10} X (cell density with microscope)−0.07541 (Fig. 1).

Regarding filters based on a library storing 100 images of *Karenia* spp., the Equivalent Spherical Diameter (ESD) ranged from 17.6 to 31.5 μm (mean ± standard deviation: 23.2±3.0786 μm) (Fig. 2). Note that the cell size can be overestimated due to fixative-induced cell swelling. The Aspect Ratio ranged from 0.62 to 0.98 (mean ± standard deviation: 0.803±0.0798). Average Green ranged from 129.47 to 163.94 (mean ± standard deviation: 151.12±7.4499). Perimeter ranged from 67.49 to 226.09 μm (mean ± standard deviation: 110.60±30.3260 μm). Circle fit ranged from 0.24 to 0.91 (mean ± standard deviation: 0.67±0.1594) (Fig. 2).

In the compiled 1000 images, tiny flagellates were dominant in number, and ciliates and dinoflagellates were abundant in a similar size range to that of *Karenia* cells (Supplementary Fig. 1). Image analysis with the FlowCam showed that the accuracy (Acu) ranged from 90 to 100% for all filter combinations (Table 1). Conversely, the True Accuracy (TAcu) varied widely, ranging from 5.52 to 55.81% (Fig. 3, Table 1). Among the single filters, ESD demonstrated the highest TAcu (19.46%), followed by Aspect Ratio (10.47%), Average Green (8.31%), Perimeter (6.95%), and Circle fit (5.52%) (Fig. 3a, Table 1). The combination of the four filters, excluding Circle fit, yielded the highest TAcu (55.81%). Filter Accuracy (FAcu) ranged from 19 to 96%, showing a similar trend to TAcu with varying filter combinations (Fig. 3b, Table 1).

Surface distribution of hydrography and *Karenia* spp

Sea surface temperatures ranged from 17.6–23.4℃, with higher values observed toward the west (Fig. 4a). Salinity ranged from 33.0–33.8, with a tendency towards higher values in the western region (Fig. 4b). Notably, all nutrients, except silicate, fell below the detection limit (nitrate < 0.1 μmol L^{-1}, nitrite < 0.05 μmol L^{-1}, ammonium < 0.10 μmol L^{-1}, phosphate < 0.05 μmol L^{-1}) (data not shown). Turbidity fluctuated between 0.99–2.92 (FTU), with an exceptional spike recorded at one station off the Kameda Peninsula, while the maximum value at other stations was 1.15 (FTU) (Fig. 4c). Fluorescence levels ranged from 0.48 to 1.7 (Fig. 4d), while the FSI varied from 1.53 to 2.00, with the highest value seen in Hakodate Bay (Fig. 4e). *Karenia* spp. were detected by microscopy at all stations, with the highest cell density observed in Hakodate Bay (23.2 cells mL^{-1}), followed by the area off the Kameda Peninsula (3.0 cells mL^{-1}) (Fig. 4f, Supplementary Table 1). Conversely, the offshore Erimo area exhibited lower densities (Fig. 4f). A similar trend in *Karenia* spp. distribution

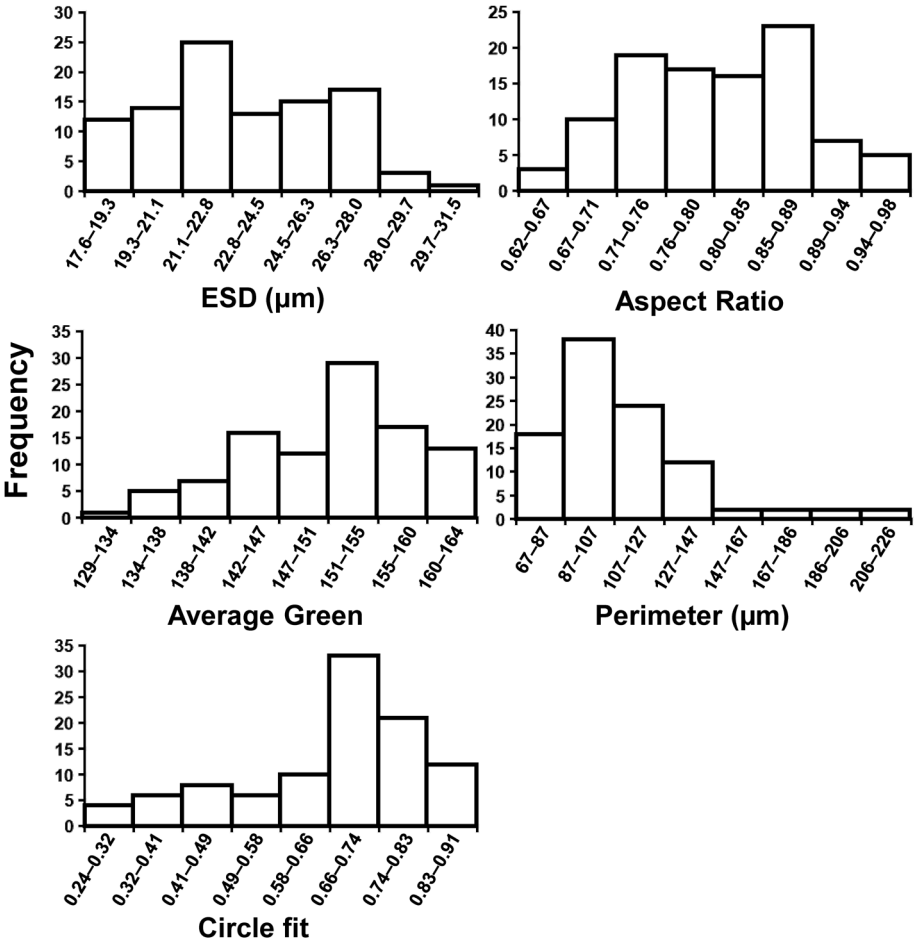

Fig. 2. The frequency of parameters in the FlowCam filter tool based on 100 images of *Karenia* spp. ESD (Equivalent Spherical Diameter), Aspect Ratio (the ratio of the major and minor axes of an ellipse centered on the particle's center of gravity), Average Green (the average intensity of green in the particle image [0–255]), Circle fit (the deviation of the particle contour from a perfect circle [perfect circle: 1]), and Perimeter (the length of the particle contour excluding the holes).

examined by the FlowCam was seen (Fig. 4g, Supplementary Table 1).

Vertical distribution of hydrography and *Karenia* spp. in Hidaka Bay

The surface layer (0–20 m depth) at the three stations (Fig. 5) showed consistent water temperatures of approximately 20℃ and salinity levels was approximately 33.5. Below 20 m depth, temperature decreased and salinity increased at the three stations. Dissolved inorganic nitrogen (DIN) and phosphate concentrations were below detection limits at the sea surface (Fig. 5). Thermo- and halo-clines were observed at approximately 20 m, with temperature and salinity gradients steeper at the St. 2, and flatter at the St. 4 (Fig. 5). Below this depth, temperature decreased, while salinity and nutrient levels increased with depth (Fig. 5). A fluorescence peak was also observed below 20 m depth. At St. 2 and 3, sampled after sunset, *Karenia* spp. exhibited high cell densities around 20 m depth, whereas at St. 4, sampled during the day, the highest cell density (1.02 cells mL^{-1}) was seen at the surface (Fig. 5).

Relationship between *Karenia* spp. and hydrography

dbRDA analysis showed that *Karenia* spp. is more likely to occur in high temperature and salinity areas (Fig. 6a). The decision tree analysis identified water temperature as a significant variable influencing suitable conditions for *Karenia* spp., with cell density showing an increase at water temperatures exceeding 20.8℃ (Fig. 6b).

Discussion

Detection of *Karenia* cells by FlowCam

The objective lens and flow cell used in this study were selected, taking into consideration the size of the *Karenia* cell. Furthermore, by establishing a threshold value for edge gradient during measurement, out-of-focus images were automatically eliminated as much as possible. Despite such meticulous settings, accurate recognition of the contours of a certain number of cells could not be accurately attained. Setting the edge gradient threshold higher increases the risk of missing images from the remaining

Table 1. Results of evaluation test using filter function in a FlowCam based on 50 correct images and 950 incorrect images from the water samples collected around Hidaka Bay during 15–18 September 2022.

Parameters					Detected numbers (N_i)	Number of correct images (N_cor)	Number of incorrect images	Accuracy (Acu)	True Accuracy (TAcu)	Filter Accuracy (FAcu)
ESD	Aspect Ratio	Average Green	Perimeter	Circle fit						
				○	851	47	804	94	5.52	19.30
			○		719	50	669	100	6.95	33.10
			○	○	604	47	557	94	7.78	44.00
		○			590	49	541	98	8.31	45.80
		○		○	533	46	487	92	8.63	50.90
		○	○		414	49	365	98	11.84	63.40
		○	○	○	370	46	324	92	12.43	67.20
	○				468	49	419	98	10.47	58.00
	○			○	450	46	404	92	10.22	59.20
	○		○		291	49	242	98	16.84	75.70
	○		○	○	284	46	238	92	16.20	75.80
	○	○			341	48	293	96	14.08	70.50
	○	○		○	326	45	281	90	13.80	71.40
	○	○	○		208	48	160	96	23.08	83.80
	○	○	○	○	202	45	157	90	22.28	83.80
○					257	50	207	100	19.46	79.30
○				○	170	47	123	94	27.65	87.40
○			○		251	50	201	100	19.92	79.90
○			○	○	169	47	122	94	27.81	87.50
○		○			158	49	109	98	31.01	89.00
○		○		○	126	46	80	92	36.51	91.60
○		○	○		156	49	107	98	31.41	89.20
○		○	○	○	126	46	80	92	36.51	91.60
○	○				102	49	53	98	48.04	94.60
○	○			○	96	46	50	92	47.92	94.60
○	○		○		100	49	51	98	49.00	94.80
○	○		○	○	95	46	49	92	48.42	94.70
○	○	○			97	48	49	96	49.48	94.90
○	○	○		○	81	45	36	90	55.56	95.90
○	○	○	○		86	48	38	96	55.81	96.00
○	○	○	○	○	81	45	36	90	55.56	95.90

ESD: Equivalent Spherical Diameter.

sharpened images. Reducing the size of the flow cell for increasing the edge gradient as much as possible for all cells raises the likelihood of cell clogging. Therefore, appropriate settings are imperative, depending on the sample condition.

The cell density of *Karenia* spp., as determined by the FlowCam, showed a positive correlation with that obtained by microscopy. However, variability increased notably at low cell densities, attributed to subsampling from the concentrated sample. Although it was not evaluated in this study, examining variations at low densities could be feasible by analyzing subsampled samples after analysis with FlowCam and counting them under a microscope. Notably, if the cell density exceeds 1 cells mL^{-1}, the FlowCam can be used to quantitatively detect *Karenia* spp. with minimal observed variation.

Image analysis using the FlowCam accurately identified over 90% of *Karenia* spp. images, while reducing non-*Karenia* spp. to a minimum of 40 or less, resulting in up to 96% Filter Accuracy (FAcu). Regarding the filter function in the FlowCam, when analyzing field samples that contain few target cells, 5% to 70% of non-target cells may be mistakenly identified as target cells (False Positive in this study) (Buskey & Hyatt 2006). Conversely, when using field samples consisting mainly of diatoms, a FAcu ranging from less than 85% to more than 90% (up to 100%) can be obtained for each species (Camoying & Yñiguez 2016). In addition, a dataset containing only images of three genera showed over 98% in Acu and TAcu (Mirasbekov et al. 2021). Compared to these previous studies, this study

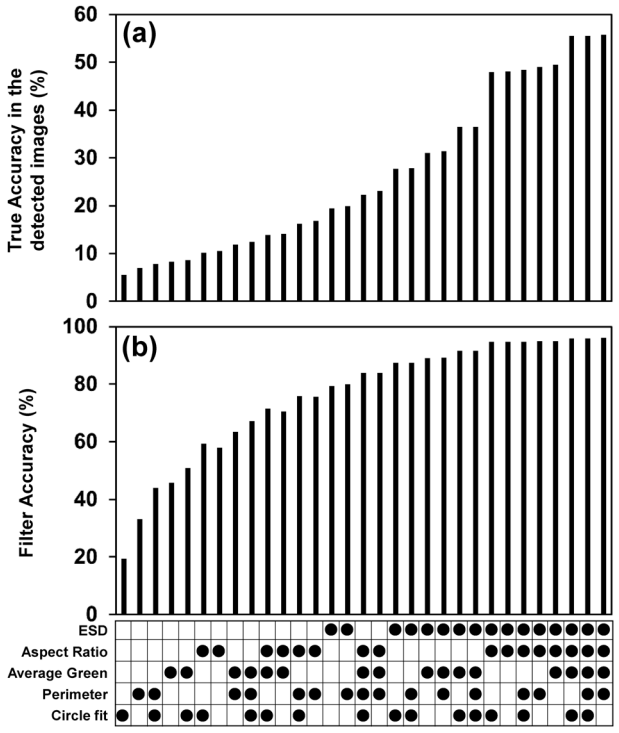

Fig. 3. True accuracy (a) and filter accuracy (b) in the classification tool in FlowCam based on 50 correct images and 950 incorrect images from the water samples collected around Hidaka Bay from 15–18 September 2022. Solid circles mean the parameter was used in the filter function. ESD: Equivalent Spherical Diameter.

exhibited good accuracy for an experiment using field samples. The classification accuracy of FlowCam's filter function is high for genera with simple morphology that do not form colonies or have protrusions (Camoying & Yñiguez 2016). *Karenia* spp. has a flattened spherical shape and does not have any protrusions, thus, its simple morphology contributed to the high accuracy reported in this study. Alternatively, species composition within the training images significantly affects classification accuracy. If another taxon with a similar spherical shape and size is contained in the training image set, the classification accuracy will decrease. In our case, low cell number in the size range of *Karenia* cells resulted in an increase in classification accuracy (Hidaka Bay in autumn). Camoying & Yñiguez (2016) conducted a similar experiment on thick disc-shaped *Coscinodiscus*, and found that Circle fit had the highest accuracy, and the lowest accuracy was when all 12 filters were combined. It is thought that the TAcu decreased because of the wide range of Circle fit values in *Karenia* images, due to misrecognition of the contours for some cells in this study's library. The same reason is why the TAcu value using Perimeter was low in this study, and the TAcu values were high when using ESD and Aspect Ratio, which are less affected by contours. Average Green enabled the exclusion of images of non-living particles, but it was unable to extract only *Karenia* images since the dataset of this study also included images of phytoplankton other than *Karenia* spp. From the above, the combination of ESD, Aspect Ratio, and Average Green is effective as a combination filter for extracting *Karenia* cells in Hidaka Bay during autumn. However, one concern about the fixation effect when imaging this species is swelling, broken cells, and bleaching. Note that our suggestion of using this combination filter and the optimum values is based on fixed samples; thus, the filters may not work well for detecting live cells. The effect of fixation in imaging by the FlowCam should be examined in the future.

While previous research has pointed out that although images can be taken with FlowCam 5–10 times faster than counting with a microscope (Buskey & Hyatt 2006), image selection may offset this advantage (Kydd et al. 2018). In this study, sample measurements were completed within 20 minutes per sample, yet manual deletion of non-living particle images consumed several hours at a maximum. Although image classification was performed manually for accuracy, utilizing the filter function can significantly reduce work flow. However, when quantifying the cell density of *Karenia* spp., if a loss of about 10% of images can be tolerated or corrected, almost all non-*Karenia* spp. images (∼95%) can be eliminated automatically by using the filter function. That will significantly reduce the work flow by FlowCam from several hours to minutes.

Distribution and expansion of *Karenia* spp. around Hidaka Bay during Autumn

Laboratory experiments using cultured strains have demonstrated that *K. mikimotoi* can grow within a water temperature range of 10–30℃ and a salinity range of 15–30, with optimal growth occurring at a water temperature 25℃ and salinity of 25 (Yamaguchi & Honjo 1989). Lam et al. (2022) also reported the ability of the Japanese strain of *K. mikimotoi* to grow at a salinity of 35. In this study, sea surface temperature ranged from 17.6–23.4℃, and salinity ranged from 33.0–33.8, indicating that the water temperature and salinity across all sampling stations fell within the conducive range for *K. mikimotoi* proliferation.

The highest cell density observed in Hakodate Bay can be attributed to the high growth rate caused by warm temperatures and physical factors such as wind currents. Notably, the growth rate of *K. mikimotoi* exhibits extreme sensitivity to temperature fluctuations within the preferred salinity range of 25 or higher (Yamaguchi & Honjo 1989). Consequently, as indicated in the decision tree analysis, the growth rate of *Karenia* spp. increases with increasing water temperatures, leading to a surge in cell numbers within Hakodate Bay. When a harmful red tide caused by *K. mikimotoi* was first recorded in Hakodate Bay in autumn 2015, high densities exceeding 100 cells mL^{-1} were predominantly concentrated in the eastern region of the bay (Shimada et al. 2016). It is believed that *K. mikimotoi* cells accumulated in the eastern part of the bay due to certain physical factors such as wind currents or estuarine circulation currents (Shimada et al. 2016). Similarly, the sampling

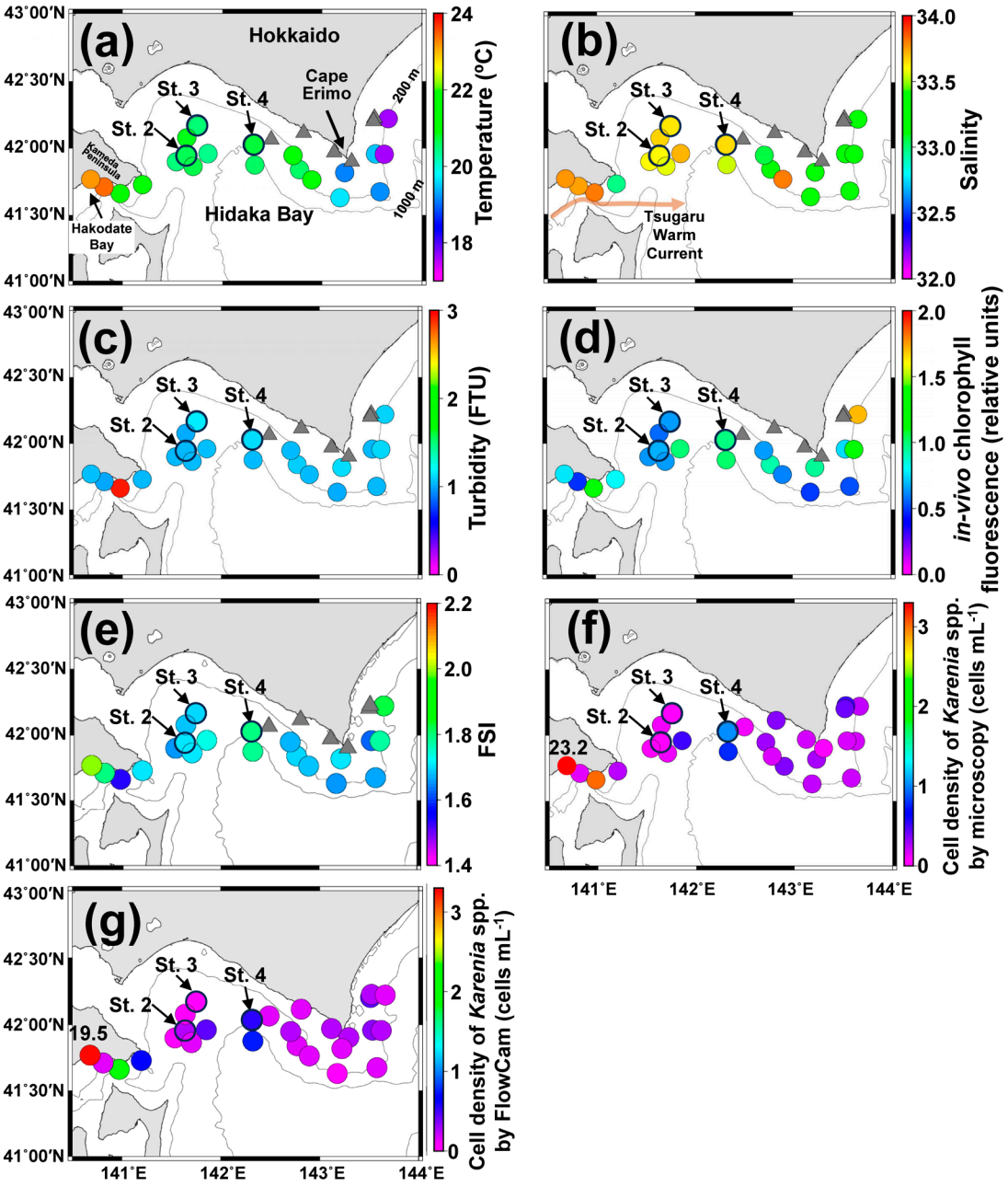

Fig. 4. Horizontal distribution of hydrography (temperature [a], salinity [b], turbidity [c], *in-vivo* chlorophyll fluorescence [d] and FSI (fluorescence spectral shift index) [e]) and cell density for *Karenia* spp. (by microscopy [f] and by FlowCam [g]) around Hidaka Bay from 15–18 September 2022. Grey triangles mean data is not available for *Ushio-Maru* cruise. Arrows and circles with solid black lines indicate stations where vertical sampling was performed using a CTD. Position of the Tsugaru Warm Current as in Yasui et al. (2022). Maximum cell density (23.2 cells mL^{-1}) of *Karenia* spp. by microscopy was found in Hakodate Bay.

station in Hakodate Bay for this study was situated in the eastern part of the bay, potentially contributing to the observed increase in *Karenia* spp. cell density resulting from cell accumulation driven by wind currents.

From September onwards, the entire area off the coast of Hidaka is occupied by Tsugaru Warm Currents water masses, persisting until winter (Ohtani et al. 1971). High-temperature, high-salinity seawater was confirmed across a wide area within Hidaka Bay in this study, indicating the influx of Tsugaru Warm Water flowing into Hidaka Bay. Shimada et al. (2016) suggested that *K. mikimotoi*, which migrated and proliferated in Hakodate Bay, may have been transported from an upstream area by the Tsugaru Warm Water. Confirming *Karenia* spp. on the sea surface at all sampling stations in this study, with higher cell density observed in the upper reaches of the Tsugaru Warm Current (i.e., Hakodate Bay) and lower density in the downstream area (offshore Erimo), supports the likelihood of transpor-

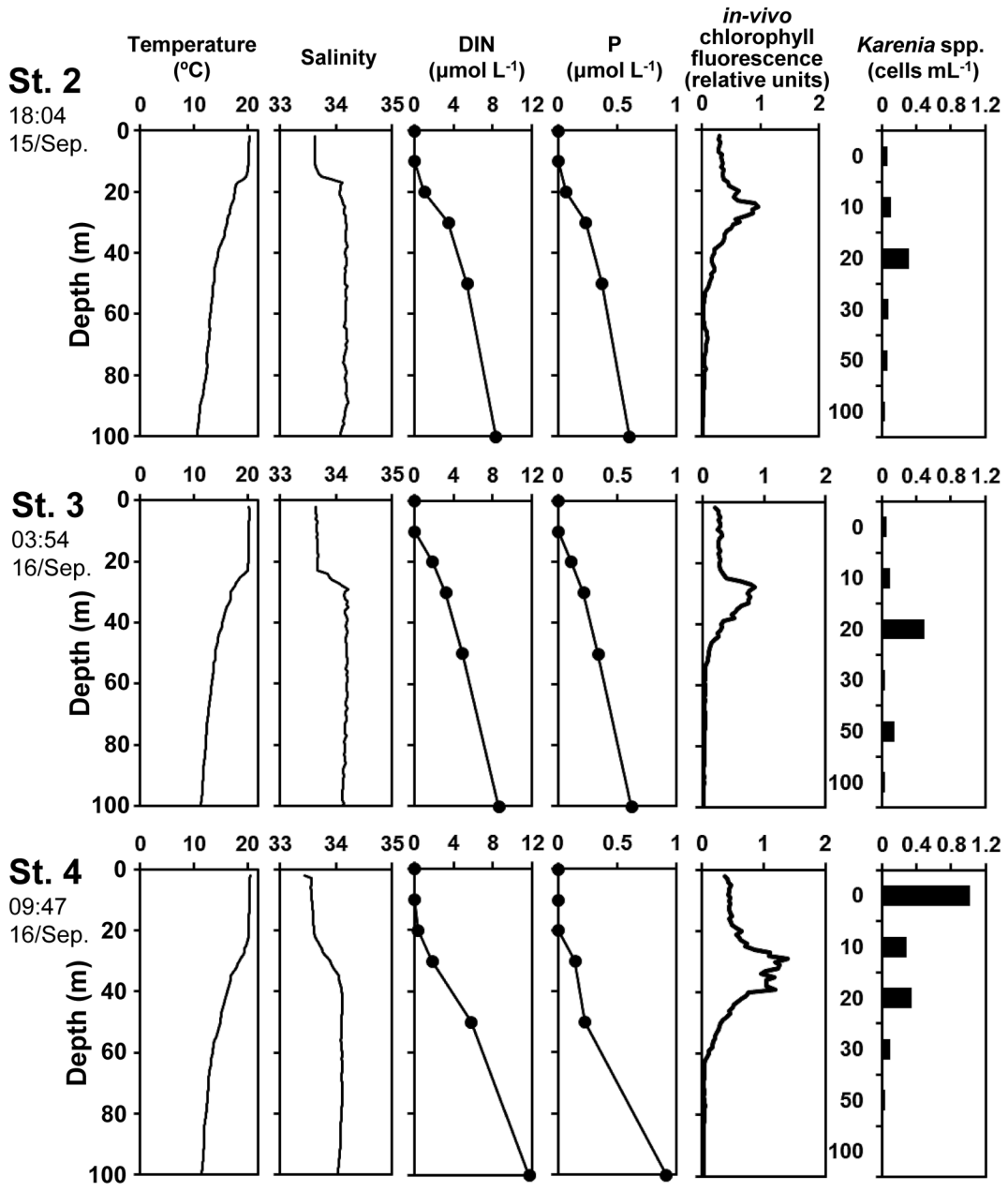

Fig. 5. Vertical changes in hydrography and cell density of *Karenia* spp. derived by microscopy around Hidaka Bay from 15–18 September 2022. The stations are referred to in Fig. 4.

tation by the Tsugaru Warm Current. Alternatively, the presence of cysts within Hakodate Bay could serve as another possible origin for this species. *Karenia mikimotoi*, being hermaphroditic, can form cysts and survive for over one year at 4ºC (Liu et al. 2020), increasing the probability of encountering gametes and producing cysts compared to dioecious species. However, these cysts are physically fragile due to their thin cell walls, and the tolerance of cysts to low temperatures has not been examined. Additionally, cysts have not been found in bottom sediments from western Japan (Imai & Itakura 1991, Shikata et al. 2008). Based on this, it is extremely unlikely that cysts exist in Hakodate Bay. Conducting genetic analysis using cultured strains from Hakodate Bay could prove effective in identifying the origin, albeit with caution due to potential genetic diversity among *K. mikimotoi* strains around Japan (Al-Kandari et al. 2011).

Considering an efficient and sustainable monitoring method for *Karenia* spp., analyses by FlowCam can be one option (Owen et al. 2022). In one study, continuous surface monitoring using the FlowCam detected a patchy distribution of harmful species (*Chattonella* spp.) in the coastal regions of western Japan (Koike et al. 2014). This system performed better than our method when a red tide occurred because cells were not affected by fixation, and there was a high spatial resolution (every minute) along a

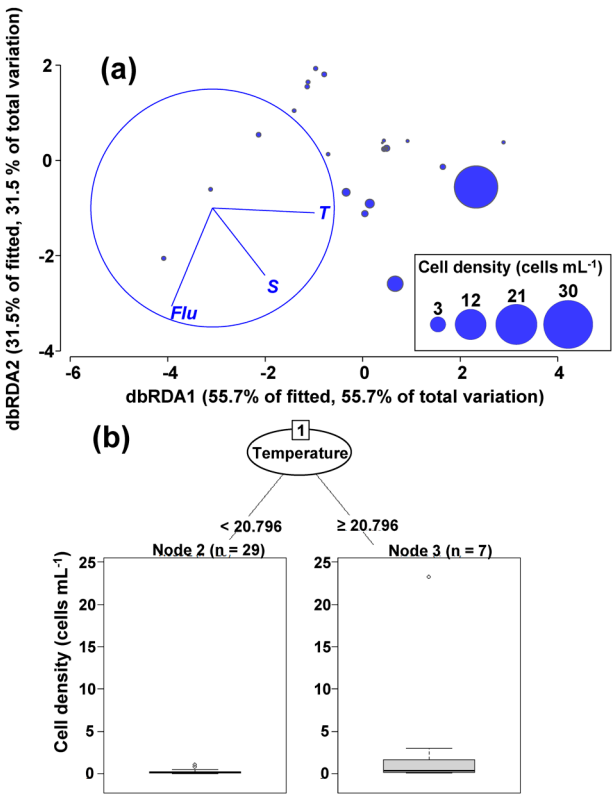

Fig. 6. dbRDA plot based on hydrographic parameters with cell density of *Karenia* spp. derived by microscopy around Hidaka Bay during 15–18 September 2022 (a). Circle size indicates the cell density. T: temperature, S: Salinity, Flu: *in-vivo* chlorophyll Fluorescence. Decision trees of cell density for *Karenia* spp. derived by microscopy around Hidaka Bay during 15–18 September 2022 (b).

148 km transect line. Conversely, the relatively new imaging instrument, PlanktoScope, should be tested for its effectiveness in phytoplankton monitoring since it is easily introduced due to the advantage of being more affordable than both the FlowCam and the imaging FlowCytobot. To apply this instrument in monitoring low-density *Karenia* distributions in broad areas, like the Pacific coastal area of Hokkaido, a surface monitoring system using both the FlowCam and PlanktoScope should be examined in the future.

Conclusion

The FlowCam demonstrates effective detection of *Karenia* spp., with sufficient quantitative ability ensured when cell density exceeds 1 cell mL^{-1}. Variations observed at low densities may stem from subsampling issues. Nevertheless, the Flowcam's automatic classification of *Karenia* spp. using the filter function yielded promising results, achieving a maximum accuracy of 96%. Specifically, the combination of ESD, Aspect Ratio, and Average Green proved effective, but note that this is based on fixed cells. While approximately 10% of *Karenia* spp. images may be lost when using the filter function, the significant reduction in workflow time required for quantifying cell density using FlowCam outweighs this drawback.

During September 2022, the entirety of Hidaka Bay and Hakodate Bay experienced water temperature and salinity conditions conducive to *K. mikimotoi* growth, with *Karenia* spp. presence confirmed at all stations. Given the stimulative effect of warm conditions on their growth rate and the inflow of the Tsugaru Warm Current into Hidaka Bay, it is plausible that *Karenia* spp. may be transported by the current from the warmer Hakodate Bay. To identify the origin of *Karenia* spp. around Hidaka Bay, a thorough investigation with strain analysis using genetic approaches is necessary. Additionally, a relatively new and inexpensive imaging instrument, the PlanktoScope, could be an option for the effective monitoring of low-density *Karenia* cells in the Pacific coastal area of Hokkaido.

Electronic supplementary material

The online version of this article (doi: 10.3800/pbr.20.1) contains supplementary material:

Supplementary Table 1. Information of surface water sampling and *Karenia* cell density using microscopy and a FlowCam around Hidaka Bay from 15–18 September 2022.

Supplementary Fig. 1. One thousand images taken by FlowCam for testing filter functions (cf. Table 1, Fig. 3). Images are arranged in order of size. White text under the photos are ESD (μm). Red lines indicate Karenia cells.

Acknowledgements

We sincerely thank Dr. Christine Weldrick for the English editing. This work was supported by the Japan Society for the Promotion of Science (JSPS) KAKENHI [grant numbers JP21H02263 (B)].

References

Al-Kandari MA, Highfield AC, Hall MJ, Hayes P, Schroeder DC (2011) Molecular tools separate harmful algal bloom species, *Karenia mikimotoi*, from different geographical regions into distinct sub-groups. Harmful Algae 10: 636–643.

Buskey EJ, Hyatt CJ (2006) Use of the FlowCAM for semi-automated recognition and enumeration of red tide cells (*Karenia brevis*) in natural plankton samples. Harmful Algae 5: 685–692.

Camoying MG, Yñiguez AT (2016) FlowCAM optimization: Attaining good quality images for higher taxonomic classification resolution of natural phytoplankton samples. Limnol Oceanogr Methods 14: 305–314.

Conlon DM (1982) On the outflow modes of the Tsugaru Warm current. La Mer 20: 60–64.

Imai I, Itakura S (1991) Importance of cysts in the population dynamics of the red tide flagellate *Heterosigma akashiwo* (Raphidophyceae). Mar Biol 133: 755–762.

Imai I, Yamaguchi M, Hori Y (2006) Eutrophication and occurrences of harmful algal blooms in the Seto Inland Sea, Japan. Plankton Benthos Res 1: 71–84.

Ito T, Togawa O, Ohnishi M, Isoda Y, Nakayama T, Shima S, Kuroda H, Iwahashi M, Sato C (2003) Variation of velocity and volume transport of the Tsugaru Warm Current in the winter of 1999–2000. Geophys Res Lett 30: 1678.

Koike K, Thaw MSH, Kitahara S (2014) On an application of FlowCam to monitor wide-range occurrence of phytoplankton: especially focusing on red-tide surveys. Bull. Plankton Soc. Japan 61: 34–40 (in Japanese with English abstract).

Kydd J, Rajakaruna H, Briski E, Bailey S (2018) Examination of a high resolution laser optical plankton counter and FlowCAM for measuring plankton concentration and size. J Sea Res 133: 2–10.

Lam W, Cheung EMS, Tam NFY, Lee TCH, Kwok CSN, Lai KKY, Xu SJ, Lee FWF (2022) Effects of Salinity on Growth and In Vitro Ichthyotoxicity of Three Strains of *Karenia mikimotoi*. J Mar Sci Eng 10: 1236.

Li X, Yan T, Lin J, Yu R, Zhou M (2017) Detrimental impacts of the dinoflagellate *Karenia mikimotoi* in Fujian coastal waters on typical marine organisms. Harmful Algae 61: 1–12.

Liu Y, Hu Z, Deng Y, Tang YZ (2020) Evidence for production of sexual resting cysts by the toxic dinoflagellate *Karenia mikimotoi* in clonal cultures and marine sediments. J Phycol 56: 121–134.

Matsuoka K, Iizuka S, Takayama H, Honjo T, Fukuyo Y, Ishimaru T (1989) Geographic distribution of *Gymnodinium nagasakiense* Takayama et Adachi around West Japan. In: Red Tides: Biology, Environmental Science, and Toxicology (eds Okaichi T, Anderson DM, Nemoto T). Elsevier, New York, pp. 101–104.

Mirasbekov Y, Zhumakhanova A, Zhantuyakova A, Sarkytbayev K, Malashenkov DV, Baishulakova A, Dashkova V, Davidson TA, Vorobjev IA, Jeppesen E, Barteneva NS (2021) Semi-automated classification of colonial *Microcystis* by FlowCAM imaging flow cytometry in mesocosm experiment reveals high heterogeneity during seasonal bloom. Sci Rep 11: 9377.

Natsuike M, Konishi T, Mizukami T (2023) Occurrences of red tides and harmful algal species in the southern Hokkaido during 2021 and 2022. Sci Rep Hokkaido Fish Res Inst 104: 53–62 (in Japanese).

Nishiyama K, Kawaguchi M, Yoshida Y, Noguchi K, Terada M, Aketagawa T, Eguchi T (2013) A red tide of Karenia mikimotoi in the Saga Imari Bay in summer, 2012. Bull Saga Genkai Fish Res Dev Cent 6: 31–62 (in Japanese with English abstract).

Ohtani K, Akiba Y, Ito E, Onoda M (1971) Studies on the change of the hydrographic conditions in the Funka Bay IV. Oceanographic condition of the Funka Bay occupied by the Tsugaru Warm Waters. Bull Fish Sci Hokkaido Univ 22: 221–230 (in Japanese with English abstract).

Olson RJ, Sosik HM (2007) A submersible imaging-in-flow instrument to analyze nano-and microplankton: Imaging FlowCytobot. Limnol Oceanogr Methods 5: 195–203.

Owen BM, Hallett CS, Cosgrove JJ, Tweedley JR, Moheimani NR (2022) Reporting of methods for automated devices: A systematic review and recommendation for studies using FlowCam for phytoplankton. Limnol Oceanogr Methods 20: 400–427.

Pollina T, Larson AG, Lombard F, Li H, Le Guen D, Colin S, de Vargas C, Prakash M (2022) PlanktoScope: affordable modular quantitative imaging platform for citizen oceanography. Front Mar Sci 9: 949428.

R Core Team, 2021. R: A language and environment for statistical computing. R Foundation for Statistical Computing, Vienna, Austria https://www.R-project.org/.

Saker ML, Neilan BA, Griffiths DJ (1999) Two morphological forms of *Cylindrospermopsis raciborskii* (cyanobacteria) isolated from Solomon Dam, Palm Island, Queensland. J Psychol 35: 599–606.

Shikata T, Nagasoe S, Matsubara T, Yoshikawa S, Yamasaki Y, Shimasaki Y, Oshima Y, Jenkinson IR, Honjo T (2008) Factors influencing the initiation of blooms of the raphidophyte *Heterosigma akashiwo* and the diatom *Skeletonema costatum* in a port in Japan. Limnol Oceanogr 53: 2503–2518.

Shimada H, Kanamori M, Yoshida H, Imai I (2016) First record of red tide due to the harmful dinoflagellate *Karenia mikimotoi* in Hakodate Bay, southern Hokkaido, in autumn 2015. Nippon Suisan Gakkaishi 82: 934−938 (in Japanese with English abstract).

Sieracki CK, Sieracki ME, Yentsch CS (1998) An imaging-in-flow system for automated analysis of marine microplankton. Mar Ecol Prog Ser 168, 285–296.

Sukhanova IN (1978) 5.2.2 Settling without the inverted microscope. In: Phytoplankton manual (eds Sournia A). United Nations Educational, Scientific and Cultural Organization, Paris, pp. 97.

Yamaguchi M, Honjo T (1989) Effects of temperature, salinity and irradiance on the growth of the noxious red tide flagellate *Gymnodinium nagasakiense* (Dinophyceae). Nippon Suisan Gakkaishi 55: 2029–2036 (in Japanese with English abstract).

Yasui T, Abe H, Hirawake T, Sasaki KI, Wakita M (2022) Seasonal pathways of the Tsugaru Warm Current revealed by high-frequency ocean radars. J Oceanogr 78: 103–119.

Yoshida M, Shimasaki Y, Inokuchi D, Nakazato A, Otake S, Qiu X, Mukai K, Foloni-Neto H, Kato H, Honda S, Oshima Y (2021) A new fluorometer to detect harmful algal bloom species and its application as a long-term HABs monitoring tool. J Fac Agr Kyushu Univ 66: 37–43.

Zuur AF, Ieno EN, Walker NJ, Saveliev AA, Smith GM (2009) Mixed effects models and extensions in ecology with R. Springer, New York.